Applied Geochemistry 113 (2020) 104496

Contents lists available at ScienceDirect

Applied Geochemistry

journal homepage: http://www.elsevier.com/locate/apgeochem

Molecular dynamics simulation of the interaction of uranium (VI) with the C–S–H phase of cement in the presence of gluconate

Iuliia Androniuk [a,*], Andrey G. Kalinichev [a,b]

[a] Laboratoire SUBATECH (UMR 6457 – Institut Mines-Télécom Atlantique, Université de Nantes, CNRS/IN2P3), 44307, Nantes, France
[b] National Research University Higher School of Economics, Russian Federation

ARTICLE INFO

Keywords:
C-S-H
Cement
Uranyl
Gluconate
Sorption
Molecular dynamics simulation

ABSTRACT

Due to their high durability and immobilization properties, cementitious materials have found a considerable application in the design and construction of radioactive waste repositories in the last decades. During cement paste production, organic additives are introduced to modify various properties of cement. The presence of such organic complexants may negatively affect the immobilizing properties of cement with respect to radionuclides. For better understanding and prediction of the effects of interactions between organic molecules and cementitious materials with radionuclides, we have developed several representative models consisting of three principal components: (i) calcium silicate hydrate (C–S–H) phase - the main binding phase of cement; (ii) gluconate, a simple well-described molecule, as a representative of organic additives; (iii) U(VI), as one of the most studied radionuclides of the actinide series. The C–S–H phase with low Ca/Si ratio (~0.83) typical for "low-pH" and degraded cement pastes has been selected for this modelling study. Structural, and energetic aspects of the sorption processes of uranyl, gluconate, and their mutual correlations on the surface of cement were quantitatively modeled by classical molecular dynamics (MD) and potential of mean force (PMF) calculations. The ternary surface complex formation between uranyl hydroxides and Ca^{2+} cations at the C–S–H aqueous interfaces is shown to have an important role in the overall sorption process. In the presence of gluconate, U(VI) sorption on C–S–H is facilitated by weakening the Ca^{2+} binding with the surface. Additionally, Na^{+} is proven to be an important competitor for certain surface sorption sites and can potentially affect the equilibrium properties of the interface.

1. Introduction

Cementitious materials are widely used in the design and construction of geological radioactive waste repositories, in particular in the Callovo-Oxfordian argillaceous rock formation in the East of the Parisian basin in France (e.g., Grambow, 2016; Kořátková et al., 2017). They are the principal construction material for the waste storage galleries and access shafts of the underground repositories, but can also serve as part of the packaging for some intermediate level waste or as the sealing material for storage cells.

Calcium silicate hydrate (C–S–H) is the main binding phase of cements and controls their mechanical and chemical durability. C–S–H phases are formed as a result of hydration of alite (Ca_3SiO_5) and industrial belite (Ca_2SiO_4), the two silicates that are the essential constituents of cement clinker (Taylor, 1997; Richardson et al., 2010). Because of its critical role, C–S–H was selected as the cement model in this work. However, an accurate nano-scale description of C–S–H phases is very challenging and the interest in understanding their atomistic structure and the nature of structural disorders continues to be strong. A significant amount of research has been devoted recently to clarify these issues using various experimental and theoretical approaches, and there is now a general consensus that the C–S–H phases have structural similarity with such minerals as tobermorite and jennite (Cong and Kirkpatrick, 1996; Yu et al., 1999; Pellenq et al., 2009; Richardson et al., 2010; Grangeon et al., 2016, 2017; Kumar et al., 2017). It is also established that Ca/Si ratio is a single most important characteristic of the C–S–H phase which significantly affects such chemical and physical properties of cement as pH of the pore water, the surface charge, and equilibrium ion concentrations (Chen et al., 2004; Lothenbach and Nonat, 2015).

The atomistic models of C–S–H used in this study to simulate the interaction of actinides with cement in the context of radioactive waste

* Corresponding author.
E-mail address: yuliya.andronyuk@gmail.com (I. Androniuk).

https://doi.org/10.1016/j.apgeochem.2019.104496
Received 29 July 2019; Received in revised form 29 November 2019; Accepted 10 December 2019
Available online 18 December 2019

repository environment were constructed on the basis of experimental observations and earlier computer simulations. They provide a compromise between the necessity to realistically represent the true compositional and structural complexity of the C–S–H phase and still maintain relative simplicity, which should facilitate better quantitative investigation of the specific molecular mechanisms of interaction among different chemical species near the surface (Androniuk et al., 2017).

The sorption behaviour of actinides on C–S–H phases has already been studied recently, and a strong effect of the Ca/Si ratio has been found (Pointeau et al., 2004; Harfouche et al., 2006; Tits et al., 2011; Gaona et al., 2012; Macé et al., 2013; Häußler et al., 2018; Tits and Wieland, 2018). Even though in ordinary Portland cement we can observe predominantly C–S–H phases with Ca/Si ratios higher than 1.5, lower ratios are typical for "low-pH" cements with added fly ash and silica fume, and in degraded cement pastes because of the decalcification (Glasser et al., 2008). As the first step, C–S–H phases with low Ca/Si ratio (~0.83) have been selected for this modelling study.

During cement paste production, various kinds of organic additives are typically used to enhance mechanical properties of the final cement material, and the presence of these potentially reactive and mobile chemicals may cause additional safety concerns (Keith-Roach, 2008). Consequently, the molecular mechanisms of their interaction with all components of the waste storage system should be systematically studied, quantitatively described, and understood in detail. Several recent studies shed light upon the behaviour of organics in cementitious materials (Nalet and Nonat, 2016; Chaudhari et al., 2017; Orozco et al., 2017) and their effect on the mobility of radionuclides in cement (Pointeau et al., 2006, 2008; García et al., 2018). However, to our knowledge, the molecular mechanisms controlling the behaviour of the ternary systems (C–S–H/radionuclide/organic) have not yet been investigated. In the present work, we are addressing this gap by atomistic computer simulations of a model ternary system. Gluconate ($C_6H_{12}O_7$) ion, a relatively simple hydroxy acid that is chemically stable in alkaline solutions, is used here as a proxy model for organic additives, while U(VI), one of the most important and well-studied actinide elements, is used as a model radionuclide.

The structural defects in the C–S–H surface silicate chains can serve as potential sorption sites for the interfacial species. The variations in structure and surface charge distribution of the C–S–H surface models create different opportunities for the cations to bind. However, not all of the binding sites are equivalent, some of them offer more favourable local steric environments and/or lower energies for stronger binding. This is where the computational molecular modelling becomes very helpful by providing a detailed quantitative atomic scale picture of the site-specific interactions on the interface. A combinational analysis of the local structures, density profiles and surface maps for target atoms gives an insight of what are the preferential sorption sites on the C–S–H surface (Androniuk et al., 2017).

A number of studies (Viallis-Terrisse et al., 2001; Hill et al., 2006; Sugiyama, 2008; Labbez et al., 2011; Bach et al., 2013; Henocq, 2017; Dufresne et al., 2018) have demonstrated that the presence of alkali on the interface of C–S–H can significantly change its equilibrium solution and surface physical and chemical properties: they can affect the surface zeta potential, compete for the sorption sites. Taking this into account consideration, Na^+ is introduced to the simulated systems as a counter ion of gluconate. The free energies of adsorption for the ions of interest (Ca^{2+}, UO_2^{2+}, gluconate, Na^+) at different surface sites of calcium silicate hydrates are calculated, analyzed, and discussed in this paper.

2. Methods

The atomistic model of the C–S–H surface for our simulations was constructed based on the crystal structure of tobermorite, that was proven to be the closest to the real cement hydrate (e.g., Grangeon et al., 2016, 2017; Kumar et al., 2017; Kunhi Mohamed et al., 2018). First, the tobermorite crystallographic unit cell ($Ca_5Si_6O_{16}(OH)_2{\cdot}4H_2O$; Hamid, 1981; Merlino et al., 2001) has been multiplied along the a and b directions (6 × 6 × 1) to create the crystal supercell of the dimensions 40.2 × 44.4 × 25.5 Å^3. This supercell was then cleaved in the middle of interlayer along the (0 0 1) crystallographic plane to create a basic model of the C–S–H surface. Next, the top layers of the cleaved crystal were modified by randomly removing the bridging Si tetrahedra in accordance with available experimental NMR and IR data (Cong and Kirkpatrick, 1996; et al., 1999; Beaudoin et al., 2009; Roosz et al., 2018), and introducing additional Ca^{2+} cations into the interlayer (Fig. 1). The protonation state of surface silanol groups was assigned based on the theoretical considerations (Churakov et al., 2014), and adjusted to correspond the range of pH ~ 10–11 typical of C–S–H with a low Ca/Si ratio. More specifically, all silanol groups of bridging Si and one of the pairing Si (replacing the introduced defect) were deprotonated. The deprotonated oxygens of the surface were assigned a partial charge of $qonb = -1.3|e|$, higher than the protonated ones in the standard ClayFF model (see Kirkpatrick et al., 2005a, 2005b, and the discussion below). The structural defects were not introduced for the silicate chains inside the bulk tobermorite substrate, since only the surface interactions are the principal focus of the present work.

The interfacial aqueous solution contained 6 ions of Na^+, $UO_2(OH)^{3-}$, and gluconate each, with ~4500 H_2O molecules, that approximately corresponds to 0.07 M ion concentrations. These relatively high concentrations had to be used in the simulations for better statistical sampling of the model systems, but they should not affect overall results. Three dimensional periodic boundary conditions (Allen and Tildesley, 2017) were applied to the constructed model interfaces, and the thickness of the solution layer between the two C–S–H surfaces was large enough (≈70 Å) to ensure that the interactions at one surface would not affect the other, and result in bulk-like solution behaviour in the middle of the model simulation box (Fig. 1).

The interatomic interaction parameters for C–S–H, H_2O, and Ca^{2+} ions were taken from the ClayFF parameterization (Cygan et al., 2004), and its later modifications for cement systems (Kirkpatrick et al., 2005b; Kalinichev et al., 2007; Mishra et al., 2017; Mutisya et al., 2017). Polarizability of actinides, such as U(VI), can generally be considered as an important factor contributing to overall interatomic interactions (Clavaguéra-Sarrio et al., 2003; Newcomb et al., 2018; Duvail et al., 2019). However, in our simulations U(VI) is only present in the form of a uranyl cation, UO_2^{2+}, and non-polarizable force field parameterization for such species has long been already proven to a be a good compromise providing accurate simulation results validated by experimental data (Guilbaud and Wipff, 1996; Greathouse et al., 2002; Kerisit and Liu, 2014). The interaction parameters for uranyl ions used in this work (Guilbaud and Wipff, 1996) are also consistent with ClayFF (Teich-McGoldrick et al., 2014).

Based on the recent comparison of several clay-organic force field combinations (Szczerba and Kalinichev, 2016), the general AMBER force field GAFF (Wang et al., 2004) was used to describe the interatomic interactions involving gluconate ions. Standard Lorenz-Berthelot mixing rules (Allen and Tildesley, 2017) were applied to calculate short-range Lennard-Jones interactions between the unlike atoms (with a cut-off distance of 14 Å). Long-range electrostatic forces were evaluated by means of the Ewald summation method. All molecular dynamics (MD) simulations were performed using LAMMPS software package (Plimpton, 1995). The Newtonian equations of atomic motions were numerically integrated with a timestep of 1 fs, and the model systems were initially equilibrated for 3 ns in the isobaric–isothermal statistical ensemble (*NPT*), then for 2 ns in the canonical ensemble (*NVT*). Temperature and pressure were constrained using the Nose-Hoover thermostat and barostat (Allen and Tildesley, 2017) at ambient conditions ($T = 300$ K, $P = 0.1$ MPa). Model equilibration was carefully monitored by assessing the temperature, pressure, kinetic and potential energy of the system, and dimensions of the simulation box, in order to confirm that these parameters reach their equilibrium steady state values on average (Braun et al., 2019).

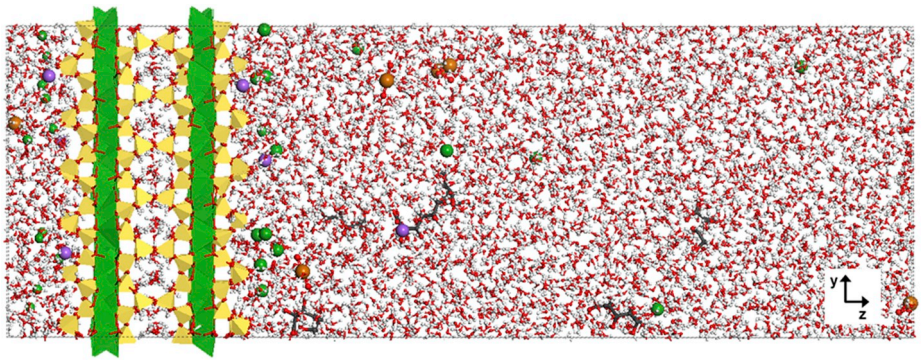

Fig. 1. A snapshot of the entire simulation supercell. The color scheme is as follows:
Si – yellow; Ca – green; O – red; H – white; Na – violet; U – dark-orange; and C – dark-grey. (For interpretation of the references to color in this figure legend, the reader is referred to the Web version of this article.)

To probe the structure of bulk aqueous solutions for comparison with the interfacial solutions, several preliminary MD simulation runs were performed for the systems containing pairs of ions ($UO_2(OH)_3^-$, Ca^{2+}, $Ca(OH)^+$, Na^+, and gluconate) placed in a cubic 40 × 40 × 40 $Å^3$ simulation box filled with H_2O molecules at a density corresponding to ambient conditions. When necessary, aqueous OH^- and Na^+ ions were added to maintain the total electrostatic neutrality of the models.

In the first series of unconstrained MD simulations, the most probable sorption sites on the C–S–H surfaces were determined based of the calculation of time-averaged atomic density profiles in the direction perpendicular to the surface, and atomic density distributions parallel to the surface in the layer of solution nearest to it. The local atomic density is calculated through the evaluation of the average number of atoms of a certain type ($\overline{N}_A$) found at a distance z (i.e, within the range of distances from z to $z + \Delta z$) parallel to the surface:

$$\text{Density}_A = \frac{\overline{N}_A \ (\Delta z)}{V_{cell}}$$

where V_{cell} is the total volume of the simulation cell, $\Delta z = 0.1$ Å. The two-dimensional distributions in the xy plane within a layer of solution parallel to the surface at a certain distance z are defined by the probability of finding an atom of type A at a position (x,y) above the surface within a range of distances from z to ($z + \Delta z$):

$$\text{Surface density}_A(x, y) = \overline{N}_A(\Delta x \Delta y)$$

where $\Delta z = 2$ to 5 Å, $\Delta x = \Delta y = 0.2$ Å.

The change of free energy is the driving force of any process, such as surface sorption. In this case, the difference in free energy between different states of the system (surface-sorbed ion *vs* the same ion in bulk aqueous solution) along a reaction coordinate can quantitatively characterize the strength of the adsorption sites of interest. Free energy is related to the probability distribution of the thermodynamic states along the reaction coordinate, and statistical analysis of an MD simulation trajectory allows one to quantitatively evaluate free energy evolution in the system using the so-called "umbrella sampling" algorithm or potential of mean force (PMF) calculation (Allen and Tildesley, 2017).

A complete calculation requires a number of separate independent simulations to cover the entire range of the reaction coordinate. In each of these "sampling windows" the distance between the reacting species is restrained at a required value using a harmonic force to allow the system to sample all possible configurations around that particular value of the reaction coordinate. The histograms of such simulation series are carefully monitored to ensure adequate and relatively uniform sampling along the reaction coordinate and sufficient overlaps of the sampling windows with each other. This ensures proper recovery of the unbiased PMF curve from the simulated ensemble of the biased histograms using the weighted histogram analysis method (WHAM). A detailed description of the umbrella sampling and WHAM algorithms used here can be found in literature (Kästner, 2011; Grossfield, 2014).

Here we additionally used the recently developed approach of site-specific PMF calculations (Loganathan and Kalinichev, 2017) where an additional weak xy constraints were applied as a "soft cylindrical wall" of a small diameter in order to keep the atom above a defined sorption site on the surface and not to allow its significant drift in the directions parallel to the surface. In this way, quantitative description of the adsorption free energy profiles was obtained for UO_2^{2+}, $UO_2(OH)_3^-$, Ca^{2+}, and Na^+ ions as functions of their distance between each other in bulk aqueous solutions, and from the C–S–H surface at the aqueous interfaces with solutions of various compositions (with and without gluconate present in the system). For each PMF curve obtained, approximately 90 constrained MD simulations (sampling windows) were run in the *NVT* ensemble (T = 300 K) for 1 ns. Monte Carlo bootstrapping approach implemented in WHAM algorithm has been used to evaluate the statistical uncertainties (Grossfield, 2014; Grossfield et al., 2018). The calculated average value of 0.02 kcal/mol is taken as an estimate of uncertainty for all PMF curves presented in this work.

3. Results and discussion

3.1. Complexation of UO_2^{2+} in aqueous solutions

Uranium (VI) exists in aqueous solutions in the form of uranyl cation, UO_2^{2+}, and in alkaline solutions it forms hydroxocomplexes of different stoichiometry with a general formula $(UO_2)_m(OH)_n^{2m-n}$ (Choppin and Mathur, 1991; Krestou and Panias, 2004; García-Hernández et al., 2006; Moll et al., 2014; Drobot et al., 2016). Hydroxyl ions in the coordination sphere of UO_2^{2+} are negatively charged, and different properties are expected for the hydrolysed species compared to the aqua complexes in solutions at lower pH. To better understand the sorption behaviour of $UO_2(OH)_3^-$ on C–S–H surfaces, a series of PMF calculations were performed for the selected pairs of ions in bulk aqueous solutions (Fig. 2).

Formation of calcium uranate carbonate complexes is known for carbonated systems (Dong et al., 2005; Fox et al., 2006; Stewart et al., 2010; Smith et al., 2015; Richter et al., 2016; Saleh et al., 2018), but in the absence of CO_2 a formation of hydroxo complexes can be suggested where cations are bound with a hydroxyl "bridge". The stabilisation by Ca^{2+} in alkaline solutions has been already proven for a number of actinides (Altmaier et al., 2008; Rabung et al., 2008; Fellhauer et al., 2010, 2016) and thus is also expected for U(VI). From the PMF profiles in Fig. 2 (a) it can be clearly seen that there is a strong interaction between aqueous $UO_2(OH)_3^-$ and Ca^{2+} ions: a stable complex is formed with the energy barrier about 10 kcal/mol. Two main energy minima found at interionic distances of ~4.1 and ~3.6 Å correspond to the formation of one and two OH^- bridges, respectively.

A fraction of calcium in alkaline solution can be present as $Ca(OH)^+$,

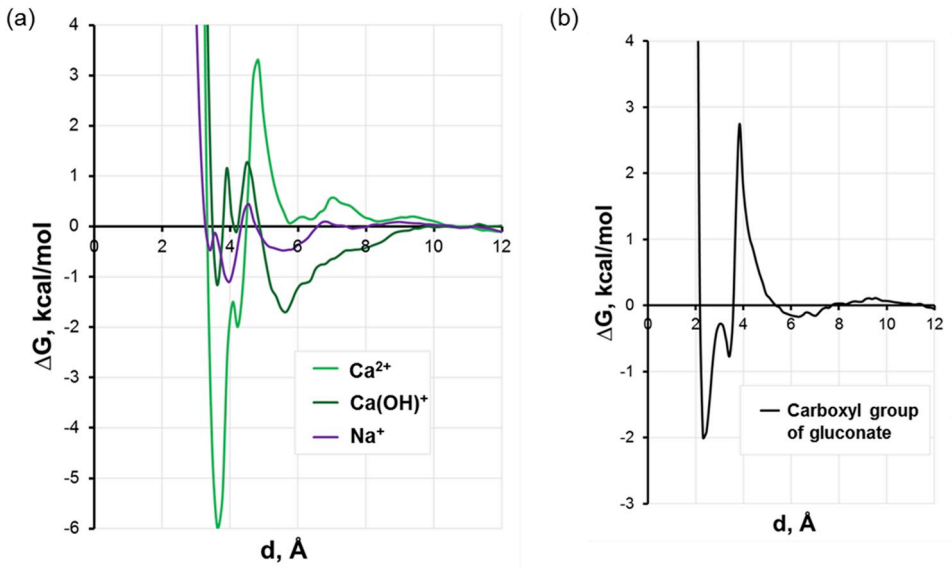

Fig. 2. The potential of mean force as a function of distance between $UO_2(OH)_3^-$ and cations (a) or carboxyl group of gluconate (b) in aqueous solution.

and a free energy profile for this pair has also been calculated. The energy minima are found at the same distance as for Ca^{2+} cation but the formed complexes have much lower stability: the energy barriers are about 2.2 kcal/mol at ~3.6 Å and 1.7 kcal/mol at 5.5 Å. Additionally, Na^+ has been studied as a potentially competitive cation that is introduced into the system as a counterion of gluconate, and it is one of the major cations present in the real cement pore water. Sodium only weakly interacts with uranyl hydroxide in water showing only two shallow minima at distances of ~3.3 and ~4.0 Å. As it can be seen, the double free energy minimum is found for all the ions studied. The complexation of U(VI) with $Ca(OH)^+$ and Na^+ can be considered weak, and these interactions should not interfere significantly with its uptake by C–S–H.

Uranyl can form complexes with more than one gluconate anion under alkaline conditions (Birjkumar et al., 2011; Colàs et al., 2013). The cation will mostly coordinate with deprotonated carboxyl groups of organic ion, but at highly alkaline solutions (pH > 13.9) the gluconate hydroxyl groups can be deprotonated and can also participate in U(VI) complexation. The plot in Fig. 2(b) shows the free energy of binding a gluconate carboxyl group to the $UO_2(OH)_3^-$ ion. Even though both ions are negatively charged, complexation is possible due to the presence of an exchangeable water molecule in the solvation shell of $UO_2(OH)_3^-$. The calculation results show that the energy required to replace this water molecule by gluconate is ~5 kcal/mol. The distinct energy minima found at ~2.5 Å ~3.4 Å corresponding to the direct binding of U(VI) to the oxygens of the carboxyl group. The difference in the distance between the two of them can be explained by the different binding configuration of the organic molecule. In addition, it was observed that these complexes are stabilised by formation of hydrogen bonds between the oxygen of aqueous OH^- ion and one or two hydrogens of the closest gluconate alcohol functional groups.

To summarize, the combination of the results for U(VI) in solution with the available literature data allows us to suggest that complex formation between uranyl hydroxides and Ca^{2+} cations present at aqueous C–S–H interfaces should play a significant role in the sorption process. Meanwhile, complexation with other interfacial ions is minor, but cannot be excluded completely.

3.2. Complexation of Ca^{2+} and Ca-gluconate at the C–S–H interface

The deprotonated silanol groups can be considered the most reactive groups of the C–S–H surface due to their high negative charge. Two typical sorption sites for Ca^{2+} on the C–S–H surface were selected for the PMF calculations in order to obtain quantitative information on the site-specific adsorption free energy: the deprotonated silanol group of the bridging silicon tetrahedron, and the deprotonated silanol group of the pairing silicon tetrahedron (the schematic representations of the sites are shown in Fig. 3).

The adsorption free energy profiles calculated for Ca^{2+} cations above two selected binding sites in Fig. 3 with and without gluconate demonstrate that in the absence of organics the energy of adsorption is nearly the same for both sorption sites sampled. The first energy minimum (at $d \approx 2.5$ Å) corresponds to the inner-sphere coordination to the deprotonated surface oxygen, while the second pronounced minimum (at $d \approx 4.2$ Å) – to the outer-sphere coordination. The energy barrier between the inner- and outer-sphere complexes is 7.5 kcal/mol for the bridging Si site and 6.5 kcal/mol for the pairing Si site. This means that the complexation of Ca^{2+} with C–S–H surface is strong and a relatively high energy is required to replace the bound cation by another ion or molecule on the site.

It is important to note that Ca^{2+} cations are not located strictly above the selected sorption sites, so the position of the first minimum does not represent the binding distance, but shows only how close the cation is to the surface on average; the z-coordinate of the deprotonated oxygen is taken as a reference of zero distance.

In our study, we consider that the cement system was equilibrated with organics prior to contact with U(VI). The C–S–H phases with low Ca/Si ratio would typically have a high number of bridging sites, therefore, these sites where selected to study the sorption of a Ca^{2+} gluconate complex in the PMF calculation, where constrains were applied only to the Ca^{2+} ion. At high pH, the formation of very stable multinuclear Ca-gluconate complexes is expected (Pallagi et al., 2014). Nevertheless, the concentrations of gluconate used here are far too low to observe such complexation. In the absence of ligand excess, cation complexation with deprotonated carboxyl group is the most probable interaction that is mostly driven by electrostatic forces.

The free energy of adsorption (dashed green line in Fig. 3) is noticeably different for Ca^{2+} when a carboxyl group of the gluconate contributes to the first coordination sphere of the cation. The first minimum at $d \approx 2.5$ Å is due to the same inner-sphere complexation as for the organic-free system, but the energy necessary to replace surface oxygen by a water molecule is lower by half in the presence of gluconate, ~2.5 kcal/mol. Also, the second energy minimum corresponding to the outer-sphere complexation disappears. Accordingly, the binding of Ca^{2+}

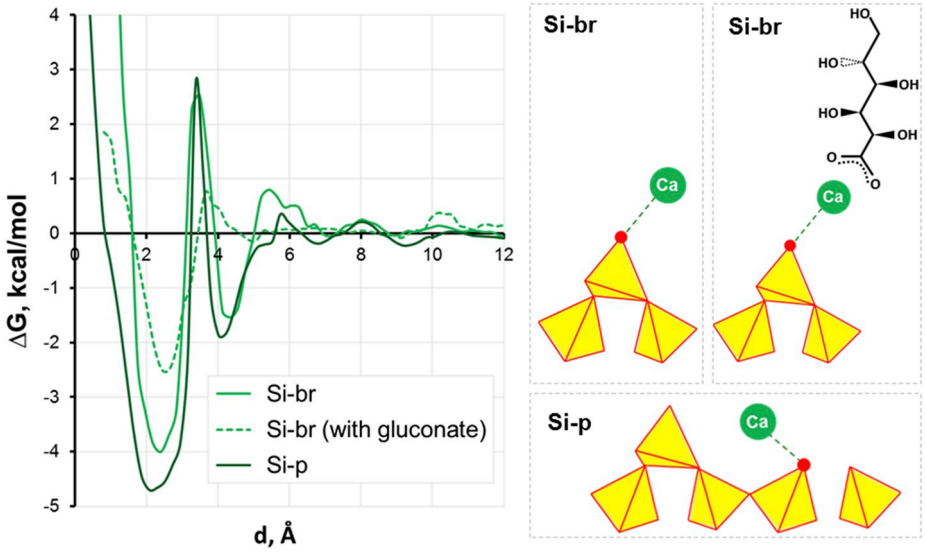

Fig. 3. Adsorption free energy profiles as functions of the distance between Ca^{2+} ion and the deprotonated silanol groups on the C–S–H surface. The schematic representation of the two distinct sorption sites (Si-br – bridging Si tetrahedron; Si-p – pairing Si tetrahedron) is shown on the right.

to the C–S–H surface becomes much weaker and potentially may result in a higher probability of substitution for a competing solution cation (e.g., Na^+ or UO_2^{2+}).

3.3. Complexation of UO_2^{2+}, $UO_2(OH)_3^-$, and Na^+ on the C–S–H surface

The MD simulations of UO_2^{2+} cations without ligands at the C–S–H surface have been performed here in order to understand the effects of aqueous hydroxyl ions and dissolved organics on the surface adsorption. UO_2^{2+} cations are bound to the same surface sites as Ca^{2+} cations and a competition between them can be expected as it was previously discussed (Androniuk et al., 2017). A preferential UO_2^{2+} sorption on the deprotonated sites is observed. The adsorption free energy profile of the uranyl cation as a function of distance from the Si-bridging site is presented in Fig. 4 (dashed line). There are two main energy minima at ~4.0 and ~6.0 Å from the surface which correspond to the formation of the inner- and outer-sphere surface complexes, respectively. Compared to Ca^{2+}, UO_2^{2+} binds farther from the surface and the energy barrier for the transition between two surface complexes is about 5.5 kcal/mol, which is 2 kcal/mol lower. UO_2^{2+} will preferably bind with the deprotonated oxygen as an inner-sphere complex on the Ca-free sites or on the sites where Ca^{2+} is sorbed as an outer-sphere complex, since the energy necessary to substitute the directly bound Ca^{2+} cation is relatively high.

The PMF oscillations seen in Fig. 4 can be associated with the local structural properties of the interface for the selected cation and sorption site: the influence of other neighboring ions, the high negative charge of the surface, and the H_2O surface rearrangements through hydrogen bonding, etc.

The general trends of $UO_2(OH)_3^-$ sorption behaviour have been first analyzed from the unconstrained MD simulations. The atomic density profiles (Fig. 5(a)) show that the closest peak for U(VI) is found at a distance of ~4–5 Å from the position of the top-most surface silanol groups. The direct binding has not been observed during the unconstrained simulations. However, the complexation of $UO_2(OH)_3^-$ with Ca^{2+} cations has been distinctly identified in the surface density maps (as illustrated in Fig. 5(b)). As expected, the PMF curve (Fig. 4) reveals

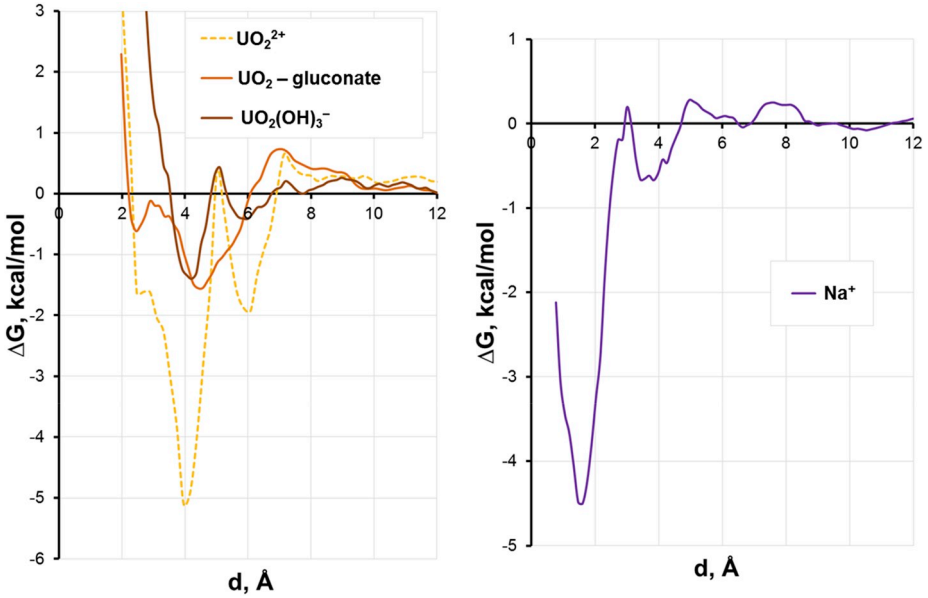

Fig. 4. Adsorption free energy profiles of uranyl (left) and Na^+ (right) as functions of their distance from the Si-bridging sorption site on C–S–H surface.

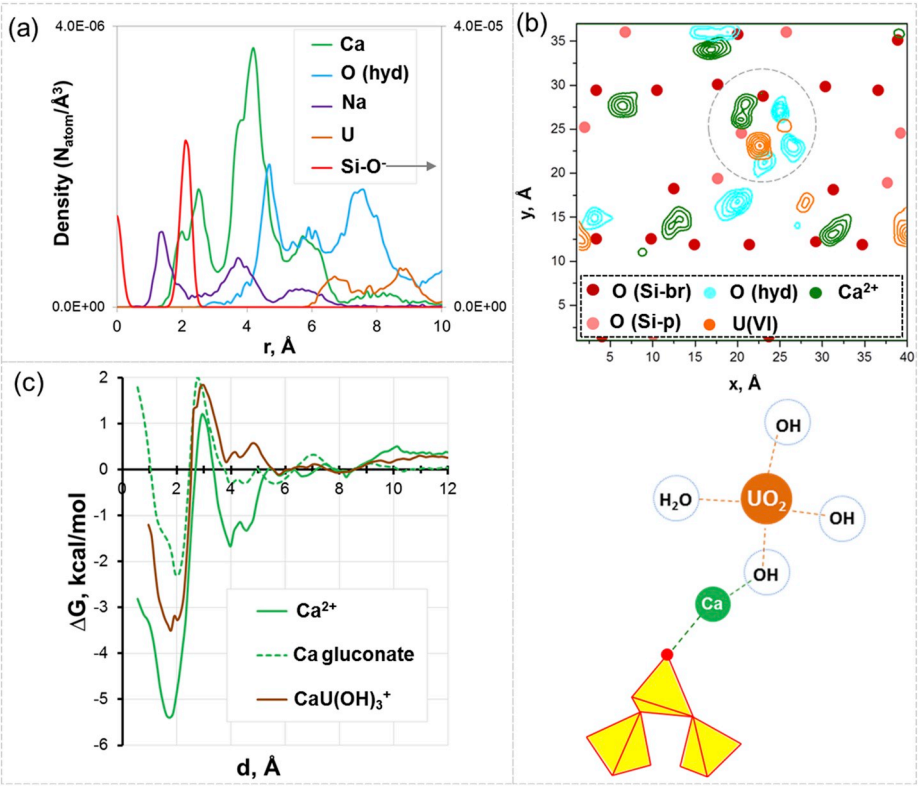

Fig. 5. Atomic density profiles of solution species near the C–S–H surface (a), atomic density contour maps of time-averaged surface distributions of selected atoms at $d \approx 4$–7 Å from the surface with the schematic representation of the surface ternary complex (b), and adsorption free energy profile of Ca complexes as functions of their distance from the Si-bridging sorption site (c).

that the sorption of $UO_2(OH)_3^-$ complex is much weaker but two distinct minima can be seen at the same distance from the Si-bridging site as for the bare UO_2^{2+} ion with the energy barriers of about ~1.8 and ~0.3 kcal/mol, respectively.

The adsorption free energy of UO_2^{2+} cation coordinated with gluconate has been calculated next (solid yellow line in Fig. 4). The free energy of adsorption of the UO_2^{2+}/gluconate complex is comparable to the one of the hydrolysed ion. However, a distinct difference in the binding energies can be observed: there is no clear separation between outer- and inner-sphere complexation with a broad shallow energy minimum found at distances $d > 4$ Å. It can be concluded that the presence of gluconate has a much more important effect on the UO_2^{2+} surface sorption, compared to Ca^{2+}, and there is more than a threefold decrease of the free energy minimum while pulling the position of the minimum further away from the surface ($d \approx 4.5$ Å).

In combination with the results from the PMF calculations in bulk solution ($UO_2(OH)_3^-/Ca^{2+}$), it would therefore be presumed that the $UO_2(OH)_3^-$ complex will preferably form a stable association with Ca^{2+} cations bound to the surface. Similar behaviour has been observed for uranyl complexation on Ca bentonite at high pH conditions (Philipp et al., 2019), where inner-sphere adsorption was found despite an anionic character of predominant aqueous species, and 4-fold coordination of U(VI) surface complexes has been proven experimentally suggesting the possible mediating contribution of Ca^{2+} cations.

Finally, the adsorption free energy of the identified $CaUO_2(OH)_3^+$ complex (Fig. 5(b)) has also been analyzed. In our model, the C–S–H surface does not have homogeneous distribution of sorption sites of the same type, so the free energy profile for an individual case will also slightly depend on the neighboring sites and sorbed cations. Thus, the PMF curves for Ca^{2+} and Ca gluconate have been analyzed for the same sorption site to provide a better reference for comparison. The main energy minima that correspond to inner-sphere complexation with the deprotonated silanol group can be found at about ~2 Å (see Fig. 5 (c)). It can be clearly seen that the sorption of $CaUO_2(OH)_3^+$ is still weaker than for Ca^{2+}, but stronger than for Ca gluconate. Thus, it can be assumed that $CaUO_2(OH)_3^+$ will become an important competitor for the sorption sites in the presence of gluconate at the interface.

It has previously been reported that U(VI) sorption is the strongest on C–S–H with lower Ca/Si ratios in the absence of alkali (Tits et al., 2011). Our present work is consistent with these results. We find that there are two main mechanisms controlling the U(VI) sorption on the C–S–H surface: the binding to unoccupied deprotonated silanols and the formation of ternary surface complex with Ca^{2+} cations. It has to be mentioned that minor fraction (<5%) of other possible species ($(UO_2(OH)_2^0$, $Ca(OH)^+$, $UO_2(OH)^+$, UO_2^{2+}, etc) will also contribute to surface sorption, even though they were not analyzed in detail in this work. For C–S–H with higher Ca/Si ratio and at higher pH, U(VI) will mostly be found as a $UO_2(OH)_4^{2-}$ complex and a larger fraction of Ca will be present as $Ca(OH)^+$. Therefore, it can be assumed that the direct binding to the surface oxygens would be less probable, and the sorption through the formation of ternary complexes will be reduced due to the less favourable binding with $Ca(OH)^+$ compared to Ca^{2+}, as it was discussed above. Several recent spectroscopic works (Tits et al., 2011, 2015; Macé et al., 2013) have shown that three distinguishable types of U(VI) species can be identified in the cementitious systems: (i) surface complexed; (ii) incorporated; (iii) precipitated. The suggested incorporated U(VI) species should not be affected by the presence of organics in the pore solution, so they were not considered in this study.

Additionally, we have analyzed the sorption of Na^+ cations on the Si-bridging site. It has been previously confirmed that the nature of interaction between alkali and C–S–H is electrostatic, and Na^+ will preferably sorb on the external surfaces of C–S–H particles (Bach et al., 2013; Henocq, 2017). In our simulations, it was observed that Na^+ cations are strongly attracted by the surface and most of them are found surface-bound for the entire time of the equilibrium MD simulation run. Na^+ has an ionic radius similar to Ca^{2+}, but its solvation shell is weaker

due to the lower charge and lower hydration energy. Thus, much less energy is required to replace a water molecule in its first coordination sphere by a negatively charged surface oxygen. It can be seen from the adsorption free energy profile (Fig. 4) that there is almost no energy barrier to overcome for Na^+ to sorb on the Si-bridging surface site. Also, the sorption behaviour of Na^+ is very similar to that of the Ca^{2+}/gluconate complex while the energy gain is almost twice as large (∼−4.5 kcal/mol for the former *vs* ∼ −2.5 for the latter). It can be concluded that Na^+ cations in solution can be very important competitors for the surface sorption sites, they are able to replace Ca^{2+} and Ca^{2+}/gluconate complex on the C–S–H surface and affect the $UO_2(OH)_3^-$ adsorption. However, the peak position of Na^+ density at the distance of ∼1–2 Å from the Si-pairing silanols shows that Na^+ is able to sorb on the sites that are less attractive for Ca^{2+}, most probably due to the difference in their charges (Fig. 5(a)). Thus, the noticeable effect of Na^+ on the sorption properties of C–S–H will be more pronounced at higher concentrations when the free sorption sites would be saturated.

4. Conclusions

The most probable mechanisms of molecular interactions in the ternary system C–S–H/U(VI)/gluconate have been quantitatively analyzed and described using classical and constrained molecular dynamics simulations. It is shown that complex formation between uranyl hydroxides and Ca^{2+} cations at the C–S–H aqueous interfaces has an important role in the overall sorption process. The existence of stable surface ternary complexes of $UO_2(OH)_3^-$ and Ca^{2+} were first identified using unconstrained MD simulations, then their adsorption free energies characterizing specific surface sites were quantitatively evaluated by the PMF calculations. Additionally, it was observed that $UO_2(OH)_3^-$ complex can bind directly to the unoccupied deprotonated surface silanols increasing its total adsorption on C–S–H surfaces with low Ca/Si ratios, which agrees well with available data in the literature.

The effect of gluconate ions on the U(VI) uptake by the C–S–H surfaces has been found to be indirect. We have shown that gluconate forms stable complexes with Ca^{2+}, decreasing the strength of its binding to the surface sorption sites. As a result, it would be easier for Ca-uranyl complexes to substitute Ca^{2+}, thus potentially increasing the uptake of U(VI) by the C–S–H phases. Finally, Na^+ is proven to be an important competitor for certain surface sorption sites and can potentially affect the equilibrium properties of the interface. However, C–S–H surfaces provide numerous other sorption sites for Na^+ ions, and the effect of the competitive alkali presence would be noticeable once these available sorption sites are occupied.

The suggested mechanisms of U(VI) sorption on the C–S–H surface with low Ca/Si ratios can be studied for other actinides that were proven to be stabilised by Ca^{2+} in alkaline solutions. C–S–H phases with low Ca/Si ratio are the model for low pH cement and degraded cements. Therefore, it is crucial to atomistically model cement at other degradation stages for the most comprehensive description of the molecular mechanisms involved in U(VI) uptake by cementitious materials. Further studies will gauge the effect of gluconate on U(VI) sorption on C–S–H phases with higher Ca/Si ratio.

Acknowledgements

The study was supported by the industrial chair “Storage and Disposal of Radioactive Waste” at the Institut Mines-Télécom Atlantique, funded by ANDRA, Orano, and EDF. A.G.K. acknowledges additional support from the HSE University Basic Research Program funded by the Russian Academic Excellence Project ‘5–100’. All calculations were performed using the supercomputing resources at CCIPL (Centre de Calcul Intensif des Pays de La Loire) and GENCI (Grand Équipement National de Calcul Intensif; projects A0020906921, A0040906921, and A0060906921). Fruitful discussions with Dr. C. Landesman (SUBATECH) and Dr. P. Henocq (ANDRA) are also gratefully acknowledged.

References

Allen, M.P., Tildesley, D.J., 2017. Computer Simulation of Liquids, second ed. Oxford University Press, New York, p. 626pp.

Altmaier, M., Neck, V., Fanghänel, T., 2008. Solubility of Zr(IV), Th(IV) and Pu(IV) hydrous oxides in $CaCl_2$ solutions and the formation of ternary Ca-M(IV)-OH complexes. Radiochim. Acta 96 (9–11), 541–550. https://doi.org/10.1524/ract.2008.1535.

Androniuk, I., Landesman, C., Henocq, P., Kalinichev, A.G., 2017. Adsorption of gluconate and uranyl on C-S-H phases: combination of wet chemistry experiments and molecular dynamics simulations for the binary systems. Phys. Chem. Earth, Parts A/B/C 99, 194–203. https://doi.org/10.1016/j.pce.2017.05.005.

Bach, T.T.H., Chabas, E., Pochard, I., Cau Dit Coumes, C., Haas, J., Frizon, F., Nonat, A., 2013. Retention of alkali ions by hydrated low-pH cements: mechanism and Na^+/K^+ selectivity. Cement Concr. Res. 51, 14–21. https://doi.org/10.1016/j.cemconres.2013.04.010.

Beaudoin, J.J., Raki, L., Alizadeh, R., 2009. A ^{29}Si MAS NMR study of modified C–S–H nanostructures. Cement Concr. Compos. 31, 585–590. https://doi.org/10.1016/j.cemconcomp.2008.11.004.

Birjkumar, K.H., Bryan, N.D., Kaltsoyannis, N., 2011. Computational investigation of the speciation of uranyl gluconate complexes in aqueous solution. Dalton Trans. 40, 11248. https://doi.org/10.1039/c1dt11086a.

Braun, E., Gilmer, J., Mayes, H.B., Mobley, D.L., Monroe, J.I., Prasad, S., Zuckerman, D. M., 2019. Best practices for foundations in molecular simulations [article v1.1]. Living J. Comput. Mol. Sci. 1 (1), 5957. https://doi.org/10.33011/livecoms.1.1.5957.

Chaudhari, O., Biernacki, J.J., Northrup, S., 2017. Effect of carboxylic and hydroxycarboxylic acids on cement hydration: experimental and molecular modeling study. J. Mater. Sci. 52, 13719–13735. https://doi.org/10.1007/s10853-017-1464-0.

Chen, J.J., Thomas, J.J., Taylor, H.F.W., Jennings, H.M., 2004. Solubility and structure of calcium silicate hydrate. Cement Concr. Res. 34, 1499–1519. https://doi.org/10.1016/j.cemconres.2004.04.034.

Choppin, G.R., Mathur, J.N., 1991. Hydrolysis of actinyl(VI) cations. Radiochim. Acta 52 (53), 25–28. https://doi.org/10.1524/ract.1991.5253.1.25.

Churakov, S.V., Labbez, C., Pegado, L., Sulpizi, M., 2014. Intrinsic acidity of surface sites in calcium silicate hydrates and its implication to their electrokinetic. properties. J. Phys. Chem. C 118, 11752–11762. https://doi.org/10.1021/jp502514a.

Clavaguéra-Sarrio, C., Hoyau, S., Ismail, N., Marsden, C.J., 2003. Modeling complexes of the uranyl ion $UO_2L_2^{n+}$: Binding energies, geometries, and bonding analysis. J. Phys. Chem. A 107 (22), 4515–4525. https://doi.org/10.1021/jp027243t.

Colàs, E., Grivé, M., Rojo, I., 2013. Complexation of uranium(VI) by gluconate in alkaline solutions. J. Solut. Chem. 42, 1545–1557. https://doi.org/10.1007/s10953-013-0048-0.

Cong, X., Kirkpatrick, R.J., 1996. ^{29}Si MAS NMR study of the structure of calcium silicate hydrate. Adv. Cem. Base Mater. 3, 144–156. https://doi.org/10.1016/S1065-7355(96)90046-2.

Cygan, R.T., Liang, J.-J., Kalinichev, A.G., 2004. Molecular models of hydroxide, oxyhydroxide, and clay phases and the development of a general force field. J. Phys. Chem. B 108, 1255–1266. https://doi.org/10.1021/jp0363287.

Dong, W., Ball, W.P., Liu, C., Wang, Z., Stone, A.T., Bai, J., Zachara, J.M., 2005. Influence of calcite and dissolved calcium on uranium(VI) sorption to a Hanford subsurface sediment. Environ. Sci. Technol. 39, 7949–7955. https://doi.org/10.1021/es0505088.

Drobot, B., Bauer, A., Steudtner, R., Tsushima, S., Bok, F., Patzschke, M., Raff, J., Brendler, V., 2016. Speciation studies of metals in trace concentrations: the mononuclear uranyl(VI) hydroxo complexes. Anal. Chem. 88, 3548–3555. https://doi.org/10.1021/acs.analchem.5b03958.

Dufresne, A., Arayro, J., Zhou, T., Ioannidou, K., Ulm, F.-J., Pellenq, R., Béland, L.K., 2018. Atomistic and mesoscale simulation of sodium and potassium adsorption in cement paste. J. Chem. Phys. 149, 074705 https://doi.org/10.1063/1.5042755.

Duvail, M., Dumas, T., Paquet, A., Coste, A., Berthon, L., Guilbaud, P., 2019. UO_2^{2+} structure in solvent extraction phases resolved at molecular and supramolecular scales: a combined molecular dynamics, EXAFS and SWAXS approach. Phys. Chem. Chem. Phys. 21, 7894–7906. https://doi.org/10.1039/C8CP07230B.

Fellhauer, D., Neck, V., Altmaier, M., Lützenkirchen, J., Fanghänel, T., 2010. Solubility of tetravalent actinides in alkaline $CaCl_2$ solutions and formation of $Ca_4[An(OH)_8]^{4+}$ complexes: a study of Np(IV) and Pu(IV) under reducing conditions and the systematic trend in the An(IV) series. Radiochim. Acta 98, 541–548. https://doi.org/10.1524/ract.2010.1751.

Fellhauer, D., Altmaier, M., Gaona, X., Lützenkirchen, J., Fanghänel, T., 2016. Np(V) solubility, speciation and solid phase formation in alkaline $CaCl_2$ solutions. Part II: thermodynamics and implications for source term estimations of nuclear waste disposal. Radiochim. Acta 104 (6), 381–397. https://doi.org/10.1515/ract-2015-2490.

Fox, P.M., Davis, J.A., Zachara, J.M., 2006. The effect of calcium on aqueous uranium (VI) speciation and adsorption to ferrihydrite and quartz. Geochem. Cosmochim. Acta 70, 1379–1387. https://doi.org/10.1016/j.gca.2005.11.027.

Gaona, X., Kulik, D.A., Macé, N., Wieland, E., 2012. Aqueous–solid solution thermodynamic model of U(VI) uptake in C–S–H phases. Appl. Geochem. 27, 81–95. https://doi.org/10.1016/j.apgeochem.2011.09.005.

García, D., Grivé, M., Duro, L., Brassinnes, S., de Pablo, J., 2018. The potential role of the degradation products of cement superplasticizers on the mobility of radionuclides. Appl. Geochem. 98, 1–9. https://doi.org/10.1016/j.apgeochem.2018.09.004.

García-Hernández, M., Willnauer, C., Krüger, S., Moskaleva, L.V., Rösch, N., 2006. Systematic DFT study of gas phase and solvated uranyl and neptunyl complexes

$[AnO_2X_4]^n$ (An = U, Np; X = F, Cl, OH, n = −2; X = H_2O, n = +2). Inorg. Chem. 45, 1356–1366. https://doi.org/10.1021/ic051492p.
Glasser, F.P., Marchand, J., Samson, E., 2008. Durability of concrete — degradation phenomena involving detrimental chemical reactions. Cement Concr. Res. 38, 226–246. https://doi.org/10.1016/j.cemconres.2007.09.015.
Grambow, B., 2016. Geological disposal of radioactive waste in clay. Elements 12, 239–245. https://doi.org/10.2113/gselements.12.4.239.
Grangeon, S., Claret, F., Roosz, C., Sato, T., Gaboreau, S., Linard, Y., 2016. Structure of nanocrystalline calcium silicate hydrates: insights from X-ray diffraction, synchrotron X-ray absorption and nuclear magnetic resonance. J. Appl. Crystallogr. 49, 771–783. https://doi.org/10.1107/S1600576716003885.
Grangeon, S., Fernandez-Martinez, A., Baronnet, A., Marty, N., Poulain, A., Elkaïm, E., Roosz, C., Gaboreau, S., Henocq, P., Claret, F., 2017. Quantitative X-ray pair distribution function analysis of nanocrystalline calcium silicate hydrates: a contribution to the understanding of cement chemistry. J. Appl. Crystallogr. 50, 14–21. https://doi.org/10.1107/S1600576716017404.
Greathouse, J.A., O'Brien, R.J., Bemis, G., Pabalan, R.T., 2002. Molecular dynamics study of aqueous uranyl interactions with quartz (010). J. Phys. Chem. B 106 (7), 1646–1655. https://doi.org/10.1021/jp013250q.
Grossfield, A., 2014. An implementation of WHAM: the weighted histogram analysis method. Version 2.0.9. http://membrane.urmc.rochester.edu/sites/default/files/wham/doc.pdf.
Grossfield, A., Patrone, P.N., Roe, D.R., Schulz, A.J., Siderius, D.W., Zuckerman, D.M., 2018. Best practices for quantification of uncertainty and sampling quality in molecular simulations [article v1.0]. Living. J. Comput. Mol. Sci. 1 (1), 5067. https://doi.org/10.33011/livecoms.1.1.5067.
Guilbaud, P., Wipff, G., 1996. Force field representation of the UO_2^{2+} cation from free energy MD simulations in water. Tests on its 18-crown-6 and NO_3^- adducts, and on its calix[6]arene^{6-} and CMPO complexes. J. Mol. Struct. THEOCHEM 366, 55–63. https://doi.org/10.1016/0166-1280(96)04496-X.
Hamid, S.A., 1981. The crystal structure of the 11Å natural tobermorite $Ca_{2.25}[Si_3O_{7.5}(OH)_{1.5}]\cdot 1H_2O$. Z. für Kristallogr. - Cryst. Mater. 154, 189–198.
Harfouche, M., Wieland, E., Dähn, R., Fujita, T., Tits, J., Kunz, D., Tsukamoto, M., 2006. EXAFS study of U(VI) uptake by calcium silicate hydrates. J. Colloid Interface Sci. 303, 195–204. https://doi.org/10.1016/j.jcis.2006.07.019.
Häußler, V., Amayri, S., Beck, A., Platte, T., Stern, T.A., Vitova, T., Reich, T., 2018. Uptake of actinides by calcium silicate hydrate (C-S-H) phases. Appl. Geochem. https://doi.org/10.1016/j.apgeochem.2018.08.021.
Henocq, P., 2017. A sorption model for alkalis in cement-based materials – correlations with solubility and electrokinetic properties. Phys. Chem. Earth, Parts A/B/C 99, 184–193. https://doi.org/10.1016/j.pce.2017.05.004.
Hill, J., Harris, A.W., Manning, M., Chambers, A., Swanton, S.W., 2006. The effect of sodium chloride on the dissolution of calcium silicate hydrate gels. Waste Manag. 26, 758–768. https://doi.org/10.1016/j.wasman.2006.01.022.
Kalinichev, A.G., Wang, J., Kirkpatrick, R.J., 2007. Molecular dynamics modeling of the structure, dynamics and energetics of mineral–water interfaces: application to cement materials. Cement Concr. Res. 37, 337–347. https://doi.org/10.1016/j.cemconres.2006.07.004.
Kästner, J., 2011. Umbrella sampling. Wiley Interdiscipl. Rev.: Comput. Mol. Sci. 1, 932–942. https://doi.org/10.1002/wcms.66.
Keith-Roach, M.J., 2008. The speciation, stability, solubility and biodegradation of organic co-contaminant radionuclide complexes: a review. Sci. Total Environ. 396, 1–11. https://doi.org/10.1016/j.scitotenv.2008.02.030.
Kerisit, S., Liu, C., 2014. Molecular dynamics simulations of uranyl and uranyl carbonate adsorption at aluminosilicate surfaces. Environ. Sci. Technol. 48 (7), 3899–3907. https://doi.org/10.1021/es405387c.
Kirkpatrick, R.J., Kalinichev, A.G., Hou, X., Struble, L., 2005. Experimental and molecular dynamics modeling studies of interlayer swelling: water incorporation in kanemite and ASR gel. Mater. Struct. 38, 449–458. https://doi.org/10.1007/BF02482141.
Kirkpatrick, R.J., Kalinichev, A.G., Wang, J., 2005. Molecular dynamics modelling of hydrated mineral interlayers and surfaces: structure and dynamics. Mineral. Mag. 69, 289–308. https://doi.org/10.1180/0026461056930251.
Kořátková, J., Zatloukal, J., Reiterman, P., Kolář, K., 2017. Concrete and cement composites used for radioactive waste deposition. J. Environ. Radioact. 178–179, 147–155. https://doi.org/10.1016/j.jenvrad.2017.08.012.
Krestou, A., Panias, D., 2004. Uranium (VI) speciation diagrams in the $UO_2^{2+}/CO_3^{2-}/H_2O$ system at 25°C. Eur. J. Miner. Process. Environ. Prot. 4, 113–129.
Kumar, A., Walder, B.J., Kunhi Mohamed, A., Hofstetter, A., Srinivasan, B., Rossini, A.J., Scrivener, K., Emsley, L., Bowen, P., 2017. The atomic-level structure of cementitious calcium silicate hydrate. J. Phys. Chem. C 121, 17188–17196. https://doi.org/10.1021/acs.jpcc.7b02439.
Kunhi Mohamed, A., Parker, S.C., Bowen, P., Galmarini, S., 2018. An atomistic building block description of C-S-H - towards a realistic C-S-H model. Cement Concr. Res. 107, 221–235. https://doi.org/10.1016/j.cemconres.2018.01.007.
Labbez, C., Pochard, I., Jönsson, B., Nonat, A., 2011. C-S-H/solution interface: experimental and Monte Carlo studies. Cement Concr. Res. 41, 161–168. https://doi.org/10.1016/j.cemconres.2010.10.002.
Loganathan, N., Kalinichev, A.G., 2017. Quantifying the mechanisms of site-specific ion exchange at an inhomogeneously charged surface: case of Cs^+/K^+ on hydrated muscovite mica. J. Phys. Chem. C 121, 7829–7836. https://doi.org/10.1021/acs.jpcc.6b13108.
Lothenbach, B., Nonat, A., 2015. Calcium silicate hydrates: solid and liquid phase composition. Cement Concr. Res. 78, 57–70. https://doi.org/10.1016/j.cemconres.2015.03.019.
Macé, N., Wieland, E., Dähn, R., Tits, J., Scheinost, A.C., 2013. EXAFS investigation on U (VI) immobilization in hardened cement paste: influence of experimental conditions on speciation. Radiochim. Acta 101, 379–389. https://doi.org/10.1524/ract.2013.2024.
Merlino, S., Bonaccorsi, E., Armbruster, T., 2001. The real structure of tobermorite 11 angstrom: normal and anomalous forms, OD character and polytypic modifications. Eur. J. Mineral. 13 (3), 577–590. https://doi.org/10.1127/0935-1221/2001/0013-0577.
Mishra, R.K., Mohamed, A.K., Geissbühler, D., Manzano, H., Jamil, T., Shahsavari, R., Kalinichev, A.G., Galmarini, S., Tao, L., Heinz, H., Pellenq, R., van Duin, A.C.T., Parker, S.C., Flatt, R.J., Bowen, P., 2017. CEMFF: a force field database for cementitious materials including validations, applications and opportunities. Cement Concr. Res. 102, 68–89. https://doi.org/10.1016/j.cemconres.2017.09.003.
Moll, H., Rossberg, A., Steudtner, R., Drobot, B., Müller, K., Tsushima, S., 2014. Uranium (VI) chemistry in strong alkaline solution: speciation and oxygen exchange mechanism. Inorg. Chem. 53, 1585–1593. https://doi.org/10.1021/ic402664n.
Mutisya, S.M., de Almeida, J.M., Miranda, C.R., 2017. Molecular simulations of cement based materials: a comparison between first principles and classical force field calculations. Comput. Mater. Sci. 138, 392–402. https://doi.org/10.1016/j.commatsci.2017.07.009.
Nalet, C., Nonat, A., 2016. Effects of functionality and stereochemistry of small organic molecules on the hydration of tricalcium silicate. Cement Concr. Res. 87, 97–104. https://doi.org/10.1016/j.cemconres.2016.06.002.
Newcomb, K., Tiwari, S.P., Rai, N., Maginn, E.J., 2018. A molecular dynamics investigation of actinyl–ligand speciation in aqueous solution. Phys. Chem. Chem. Phys. 20, 15753–15763. https://doi.org/10.1039/C8CP01944D.
Orozco, C.A., Chun, B.W., Geng, G., Emwas, A.H., Monteiro, P.J.M., 2017. Characterization of the bonds developed between calcium silicate hydrate and polycarboxylate-based superplasticizers with silyl functionalities. Langmuir 33, 3404–3412. https://doi.org/10.1021/acs.langmuir.6b04368.
Pallagi, A., Bajnóczi, E.G., Canton, S.E., Bolin, T., Peintler, G., Kutus, B., Kele, Z., Pálinkó, I., Sipos, P., 2014. Multinuclear Complex Formation between Ca(II) and Gluconate Ions in Hyperalkaline Solutions. Environ. Sci. Technol. 48 (12), 6604–6611. https://doi.org/10.1021/es501067w.
Pellenq, R.J.-M., Kushima, A., Shahsavari, R., Van Vliet, K.J., Buehler, M.J., Yip, S., Ulm, F.-J., 2009. A realistic molecular model of cement hydrates. Proc. Natl. Acad. Sci. 106, 16102–16107. https://doi.org/10.1073/pnas.0902180106.
Philipp, T., Aldin Azzam, S.S., Rossberg, A., Huittinen, N., Schmeide, K., Stumpf, T., 2019. U(VI) sorption on Ca-bentonite at (hyper)alkaline conditions – spectroscopic investigations of retention mechanisms. Sci. Total Environ. 676, 469–481. https://doi.org/10.1016/j.scitotenv.2019.04.274.
Plimpton, S., 1995. Fast parallel algorithms for short-range molecular dynamics. J. Comput. Phys. 117, 1–19. https://doi.org/10.1006/jcph.1995.1039.
Pointeau, I., Landesman, C., Giffaut, E., Reiller, P., 2004. Reproducibility of the uptake of U(VI) onto degraded cement pastes and calcium silicate hydrate phases. Radiochim. Acta 92, 645–650. https://doi.org/10.1524/ract.92.9.645.55008.
Pointeau, I., Hainos, D., Coreau, N., Reiller, P., 2006. Effect of organics on selenite uptake by cementitious materials. Waste Manag. 26, 733–740. https://doi.org/10.1016/j.wasman.2006.01.026.
Pointeau, I., Coreau, N., Reiller, P.E., 2008. Uptake of anionic radionuclides onto degraded cement pastes and competing effect of organic ligands. Radiochim. Acta 96, 367–374. https://doi.org/10.1524/ract.2008.1503.
Rabung, T., Altmaier, M., Neck, V., Fanghänel, T., 2008. A TRLFS study of Cm(III) hydroxide complexes in alkaline $CaCl_2$ solutions. Radiochim. Acta 96, 551–559. https://doi.org/10.1524/ract.2008.1536.
Richardson, I.G., Skibsted, J., Black, L., Kirkpatrick, R.J., 2010. Characterisation of cement hydrate phases by TEM, NMR and Raman spectroscopy. Adv. Cem. Res. 22, 233–248. https://doi.org/10.1680/adcr.2010.22.4.233.
Richter, C., Müller, K., Drobot, B., Steudtner, R., Großmann, K., Stockmann, M., Brendler, V., 2016. Macroscopic and spectroscopic characterization of uranium(VI) sorption onto orthoclase and muscovite and the influence of competing Ca^{2+}. Geochem. Cosmochim. Acta 189, 143–157. https://doi.org/10.1016/j.gca.2016.05.045.
Roosz, C., Vieillard, P., Blanc, P., Gaboreau, S., Gailhanou, H., Braithwaite, D., Montouillout, V., Denoyel, R., Henocq, P., Madé, B., 2018. Thermodynamic properties of C-S-H, C-A-S-H and M-S-H phases: results from direct measurements and predictive modelling. Appl. Geochem. 92, 140–156. https://doi.org/10.1016/j.apgeochem.2018.03.004.
Saleh, A.Sh, Lee, J.-Y., Jo, Y., Yun, J.-I., 2018. Uranium(VI) sorption complexes on silica in the presence of calcium and carbonate. J. Environ. Radioact. 182, 63–69. https://doi.org/10.1016/j.jenvrad.2017.11.006.
Smith, K.F., Bryan, N.D., Swinburne, A.N., Bots, P., Shaw, S., Natrajan, L.S., Mosselmans, J.F.W., Livens, F.R., Morris, K., 2015. U(VI) behaviour in hyperalkaline calcite systems. Geochem. Cosmochim. Acta 148, 343–359. https://doi.org/10.1016/j.gca.2014.09.043.
Stewart, B.D., Mayes, M.A., Fendorf, S., 2010. Impact of uranyl−calcium−carbonato complexes on uranium(VI) adsorption to synthetic and natural sediments. Environ. Sci. Technol. 44, 928–934. https://doi.org/10.1021/es902194x.
Sugiyama, D., 2008. Chemical alteration of calcium silicate hydrate (C–S–H) in sodium chloride solution. Cement Concr. Res. 38, 1270–1275. https://doi.org/10.1016/j.cemconres.2008.06.002.
Szczerba, M., Kalinichev, A.G., 2016. Intercalation of ethylene glycol in smectites: several molecular simulation models verified by X-ray diffraction data. Clay Clay Miner. 64, 488–502. https://doi.org/10.1346/CCMN.2016.0640411.
Taylor, H.F.W., 1997. Cement Chemistry, second ed. Thomas Telford, p. 459.

Teich-McGoldrick, S.L., Greathouse, J.A., Cygan, R.T., 2014. Molecular dynamics simulations of uranyl adsorption and structure on the basal surface of muscovite. Mol. Simul. 40, 610–617. https://doi.org/10.1080/08927022.2013.838675.

Tits, J., Geipel, G., Macé, N., Eilzer, M., Wieland, E., 2011. Determination of uranium(VI) sorbed species in calcium silicate hydrate phases: a laser-induced luminescence spectroscopy and batch sorption study. J. Colloid Interface Sci. 359, 248–256. https://doi.org/10.1016/j.jcis.2011.03.046.

Tits, J., Walther, C., Stumpf, T., Macé, N., Wieland, E., 2015. A luminescence line-narrowing spectroscopic study of the uranium(VI) interaction with cementitious materials and titanium dioxide. Dalton Trans. 44 (3), 966–976. https://doi.org/10.1039/c4dt02172j.

Tits, J., Wieland, E., 2018. Actinide Sorption by Cementitious Materials (PSI Bericht No. 18-02). Paul Scherrer Institut (PSI).

Viallis-Terrisse, H., Nonat, A., Petit, J.-C., 2001. Zeta-potential study of calcium silicate hydrates interacting with alkaline cations. J. Colloid Interface Sci. 244, 58–65. https://doi.org/10.1006/jcis.2001.7897.

Wang, J., Wolf, R.M., Caldwell, J.W., Kollman, P.A., Case, D.A., 2004. Development and testing of a general AMBER force field. J. Comput. Chem. 25, 1157–1174. https://doi.org/10.1002/jcc.20035.

Yu, P., Kirkpatrick, R.J., Poe, B., McMillan, P.F., Cong, X.D., 1999. Structure of calcium silicate hydrate (C-S-H): near-, mid-, and far-infrared spectroscopy. J. Am. Ceram. Soc. 82, 742–748. https://doi.org/10.1111/j.1151-2916.1999.tb01826.x.